International Journal of New Horizons in Physics

http://dx.doi.org/10.12785/ijnhp/020201

Relative Intensity Noise and Nonlinear Distortions of Semiconductor laser under Analog Modulation for Use in CATV Systems

Safwat W. Z. Mahmoud[1,*] ***and Alaa Mahmoud***[2]

[1]Department of Physics, Faculty of Science, Minia University, 61519 El-Minia, Egypt.
[2]High Institute for Engineering and Technology, El-Minia, Egypt.

Received: 04 Nov. 2014, Revised: 25 Dec. 2014, Accepted: 28 Feb. 2015
Published online: 1 Jul. 2015

Abstract: This paper presents numerical modeling of noise and distortion of semiconductor lasers subject to two-tone modulation for use in the cable television (CATV) systems. The waveform of the laser signal is simulated over wide ranges of the modulation index and placements of the modulation channel. The power spectrum and the frequency spectrum of the relative intensity noise (RIN) are characterized, and the associated second-order harmonic distortion (2HD), and the second-order (IMD2) and third-order intermodulation distortions (IMD3) are calculated. The calculated data are used to predict the measures of the CATV system performance. The dynamic range of linearity of the laser is evaluated in terms of the spurious free dynamic range (SFDR). We show that under weak modulation, the low-frequency RIN is constant at -168 dB/Hz regardless the modulation frequency. Within this accepted noise level, IMD2 is 4 dBm higher than 2HD and 10 dBm higher than IMD3. When the modulation index exceeds 25%, the laser emits clipped signals associated with large values of signal distortions. Accepted noise and distortion values correspond to lower modulation index and /or modulation channel frequency.

Keywords: Distortion; Intensity modulation; CATV; Semiconductor laser.

1 Introduction

As the light-wave technology has begun to penetrate closer to the subscriber, there has been an intensive interest in the cost-effective transmission of TV signals [1]. The optical transmission technology was introduced to the CATV system [2]. The analog CATV system using semiconductor laser diodes (SLs) has great advantages as to cost, compatibility with existing equipment, and signal quality [1]. These are the most important criteria in the directly modulated optical fiber links [1].

However, directly modulated SL introduces high intensity noise and nonlinear distortions due to its inherent characteristics [3,4], for instant the nonlinear carrier-photon resonance, which limit the transmission performance of SLs. When the SL is directly modulated by RF signals and even if the lasing power changes linearly with the injection current, there exist intrinsic nonlinear fluctuations of the electron and photon densities in the active region. These nonlinearities produce nonlinear distortion products in the modulated laser signal [3].

The main distortion types are the harmonic distortions (HDs) and intermodulation distortions (IMDs). While HD is a single-tone distortion product, IMD is a multi-tone distortion product induced when two or more signals are present at the input of the laser. Analysis of several stimulus tones can become very complex, so it is a common practice to limit the analysis to two tones. When the laser is modulated with two frequencies f_1 and f_2, the 2^{nd}-order intermodulation products would occur at $f_1 + f_2$ and $f_2 - f_1$, whereas the 3^{rd}-order intermodulation products occur at $2f_1 \pm f_2$ and $2f_2 \pm f_1$ [5]. IMD3 determines the SFDR of the laser diode, which is defined as the power difference between the signal and the noise floor when the IMD3 power is equal to the noise floor [6].

In CATV systems, it is essential to minimize the noise and distortions to enlarge the channel capacity and increase the picture quality [7]. Figures of merit in the CATV technology include the carrier-to-noise ratio

* Corresponding author e-mail: safwatwilliam@yahoo.com

(CNR), composite second order (CSO) and composite triple beat (CTB) distortions. CNR should exceed 50 dBc [1,8,9] in order to avoid the interference of noise with the signal, or the so-called "snow" that can overwhelm the picture resolution and contrast [10]. CNR is strongly influenced by RIN of the source laser [11,12,13,14,15]. Brillant [8] and Darcie et al. [9] showed that RIN of -155 dB/Hz or better is required to improve the CNR, whereas other researches confirmed that it should be less than -160 dB/Hz [16,17].

On the other hand, degrading CSO below -60 dBc and CTB below -65dBc [2,18] cause the TV picture to appear by undesired tilted lines [8,10]. CSO and CTB can be measured indirectly by the two-tone test by summing all second and third order intermodulation distortion products falling in a certain channel, respectively [11,18]. Lu et al. [12] confirmed that the reduced 2HD/IMD3 values subsequently improve the CSO/CTB values. A typical problem in the design of a CATV system is to optimize the values of CNR, CSO and CTB simultaneously [4]. While the modulation index is preferred to be as large as possible to reduce the negative impact of the laser RIN [4,8,11], it should be fundamentally limited to avoid the nonlinear distortions [4,7,10]. When the modulation current exceeds the laser threshold, it induces signal clipping [11,13,14,15].

The channels position is another important issue for the quantification of the distortion effects. Ackemn et al [17] confirmed that high-frequency channels suffer greater distortion than lower-frequency channels. Helms [18] showed that both IMD2 and IMD3 increase with the increase in the modulation frequency reaching a maximum near the relaxation oscillation frequency. Therefore, allocating a balance range between laser noise and nonlinear distortion products is necessary for better performance of the directly modulated CATV systems [4].

In this paper, we introduce comprehensive simulations of the laser noise and nonlinear distortions modulated by arbitrarily placed two-adjacent frequencies according to the standard National Television Standards Committee (NTSC) plan for the CATV signal transport. We investigate the optimum range of the modulation index that corresponds to low noise, high CNR and low distortion products. We discuss the relationship of the simulation results with both CSO and CTB distortions, which help CATV system designers to choose the optimal operation conditions with high-signal quality. This study is based on numerical integration of the rate equation model of SLs under two-tone modulation [14].

We newly characterize the two-tone modulated laser signal in both the time and frequency domains. The time domain characteristics include the waveform and the associated nonlinear distortion products, including 2HD, IMD2 and IMD3. The frequency domain characteristics include the power spectrum and the associated RIN as well as CNR. We also calculate the SFDR of the investigate laser diode and elucidate its relation to the position of the modulation channel. We show that when $m \leq 20\%$, RIN is almost constant at -168 dB/Hz and CNR increases from 55 dBc to 80 dBc due to an increase in the fundamental amplitude. Under stronger modulation, the signal is clipped, and all distortion types increase with the increase in the modulation index and /or modulation channel frequency, which predicts an increase in the CSO and CTB distortions in multichannel systems.

2 Theoretical Model

The dynamic behavior and modulation characteristics of SLs are modeled by the following pair of rate equations of the photon density $S(t)$ and injected carrier density $N(t)$ with modulation current $I(t)$ [19]

$$\frac{dS}{dt} = \frac{\Gamma g_0(N(t)-N_0)}{1+\varepsilon S(t)}S(t) - \frac{S(t)}{\tau_p} + \frac{\Gamma\beta N(t)}{\tau_c} + F_S(t) \quad (1)$$

$$\frac{dN}{dt} = \frac{I(t)}{eV} - \frac{N}{\tau_c} - \frac{g_0(N(t)-N_0)}{1+\varepsilon S(t)}S(t) + F_N(t) \quad (2)$$

where Γ is the confinement factor, N_0 is carrier density at transparency, β is the fraction of spontaneous emission noise coupled into the lasing mode, g_0 is the differential gain coefficient, ε is the nonlinear gain compression factor, τ_p is the photon lifetime, τ_c is the carrier lifetime and V is the active layer volume. The output power $P(t)$ is related to the emitted photon density $S(t)$ through the relationship:

$$P(t) = \frac{V\eta\nu}{2\Gamma\tau_p}S(t) \quad (3)$$

where η is the deferential quantum efficiency, ν is the optical frequency and h is the Planck's constant. The injection current $I(t)$ is given by:

$$I(t) = I_b + I_m \times \Psi_m(t) \quad (4)$$

where I_b is the bias current, I_m is the modulation current, and represents the shape of the electrical current signal. In the two-tone modulation of the analog NTSC system, two sinusoidal carriers of frequencies f_{m1} and f_{m2} (50 - 550 MHz) at bandwidth for each 6 MHz is generated according to:

$$\Psi_m(t) = A\sin(2\pi f_{m1}) + A\sin(2\pi f_{m2}) \quad (5)$$

where A is the amplitude. The modulation index (m) is defined as [8]

$$m\% = \frac{A \times I_m}{I_b} \times 100 \quad (6)$$

The last terms F_S and F_N in rate Eqs.1 and 2 are Langevin noise sources with zero mean values, and are added to the equations to account for intrinsic fluctuations of the laser [20]. The spectrum of RIN is defined as the Fourier transform of the auto-correlation functions of the signal power $P(t)$:

$$RIN = \frac{1}{\overline{P}^2}\int_0^\infty \delta P(t)\delta P(t+\tau)e^{j\omega\tau}d\tau \quad (7)$$

where ω is the Fourier angular frequency. For integration of the rate equations over a long time period T, RIN is calculated as [21]

$$RIN = \frac{1}{\overline{P}^2}\{\frac{1}{T}\int_0^T[\int_0^\infty \delta P(t)\delta P(t+\tau)e^{j\omega\tau}d\tau]dt\} = \frac{1}{\overline{P}^2}\{\frac{1}{T}|\int_0^T \delta P(t)e^{j\omega\tau}d\tau|^2\} \quad (8)$$

3 Calculation procedures

Rate equations (1) and (2) are numerically integrated using the 4^{th}-otder Runge-Kutta method using a fine time step of $\triangle t \sim 5$ ps. The time trajectories of $S(t)$ and $N(t)$ are evaluated over long period expending more than 512 cycles of period $T_m = 1/f_m$. The power spectrum $p(\omega)$ of the laser output is calculated from the time trajectory $S(t)$ by using the FFT of $S(t)$ as [20].

$$p(\omega) = \sqrt{\frac{\triangle t}{T}}|FFT(S(t))| \quad (9)$$

In this calculation, the longer half of the time trajectory of $P(t)$ is considered, which ascertains that the laser transients are discarded and the laser output is stabilized [22]. The values of the parameters used in the calculations are defined in table(1). These parameters stand for Distributed Feedback (DFB) lasers. The simulations are done by setting I_b and A at fixed values and varying the modulation current Im.

Table 1: Values of DFB laser parameters used in the calculations.

Symbol	Definition	Value
λ	Wavelength	$1.55nm$
V	Active layer volume	$1.5x10^{-10}cm^3$
η	Quantum efficiency	0.4
g_0	Differential gain coefficient	$2.5x10^{-16}cm^2$
N_0	Carrier density at transparency	$1.0x10^7cm^{-3}$
Γ	Mode confinement factor	0.4
τ_c	Carrier lifetime	$1.0x10_{-9}s$
τ_p	Photon lifetime	$3.0x10_{-12}s$
β	Spontaneous emission factor	$3.0x10_{-5}$
ε	Gain compression coefficient	$1x10^{-17}cm^3$
α	Linewidth enhancement factor	5
I_{th}	Threshold current	$33.45mA$
I_b	Bias current	$60mA$

Figure (1) depicts a typical simulated scheme of the modulation response of the laser under two-tone modulation. The second order intermodulation products occur at $f_1 + f_2$ and $f_2 - f_1$, whereas the third order intermodulation products occur at $2f_1 \pm f_2$ and $2f_2 \pm f_1$ [5]. We calculate the nearest products to the interested two channels, where the components $f_1 + f_2$, $2f_1 + f_2$ and $2f_2 + f_1$ are out of the band. The CNR and the distortion products 2HD, IMD2 and IMD3 of are evaluated from this figure as follows. We calculate the fast Fourier transformation (FFT) of the modulated signal, and pick up both the fundamental amplitude at f_{m1} (the TV channel's visual carrier) and the noise floor in specified bandwidth centered within the cable television channel. CNR (in dBc) is then calculated as the difference between both power levels in decibels dB [1,11]. The peak amplitudes of the fundamental carrier and the higher harmonic products are recorded. Then the difference between the peak of the 2^{nd} order harmonic and the carrier level represents 2HD, whereas the differences between the distortion peaks of the second and 3^{rd} order intermodulation components and the carrier level measure IMD2 and IMD3, respectively.

4 Results and Discussion

4.1 Noise characteristics

The noise sources that limit the total CNR include thermal noise and shot noise in the optical receiver, and the RIN of the laser [9]. Analog lasers should be chosen on the basis of optimum RIN [11,12,13,14,15]. We characterize the laser noise in terms of the spectral characteristic of RIN and its level in the low-frequency regime, LF-RIN. In figure (2), we plot the LF-RIN level as a function of the modulation index m. The laser is modulated by the two frequencies $f_{m1} = 367.25$ MHz (ch. 48) and $f_{m2} = 373.25$ MHz (ch. 49). The three insets (a)-(c) are plots of the frequency spectra of RIN at three distinct indices $m = 10\%$ (weak modulation), 35% (intermediate modulation), and 80% (strong modulation). As shown in figure(2), LF-RIN is almost constant at -168 dB/Hz when $m \leq 20\%$. In this case, inset (a) shows that the RIN spectrum is characterized by two sharp peaks at the two closed frequencies f_{m1} and f_{m2}. The spectrum displays also a peak at the relaxation frequency of the laser, f_r = 4.7 GHz. The low-frequency part of the spectrum is almost flat (white noise) at LF-RIN = -168 dB/Hz. When m increases beyond 20%, LF-RIN degrades to higher values. When $m = 35\%$, the LF-RIN reaches the threshold acceptable LF-RIN values,< -155 dB/Hz according to [9,11]. Inset (b) shows that that the RIN spectrum has sharp peaks at f_{m1} and f_{m2} as well as their higher harmonics, which indicates existence of harmonic distortion. The further increase in m induces much more degradation in the LF-RIN level. Inset (c) shows a chaos-like RIN, which is manifestation of the completely distorted signal in this case of strong modulation, $m = 80\%$. These noise characteristics are in qualitative fit with the results predicted by Ahmed et al. [23] for single-tone modulation of laser diodes.

In figure (3), we plot variation of the LF-RIN in the regimes of weak modulation (m =5, 10, and 20%),

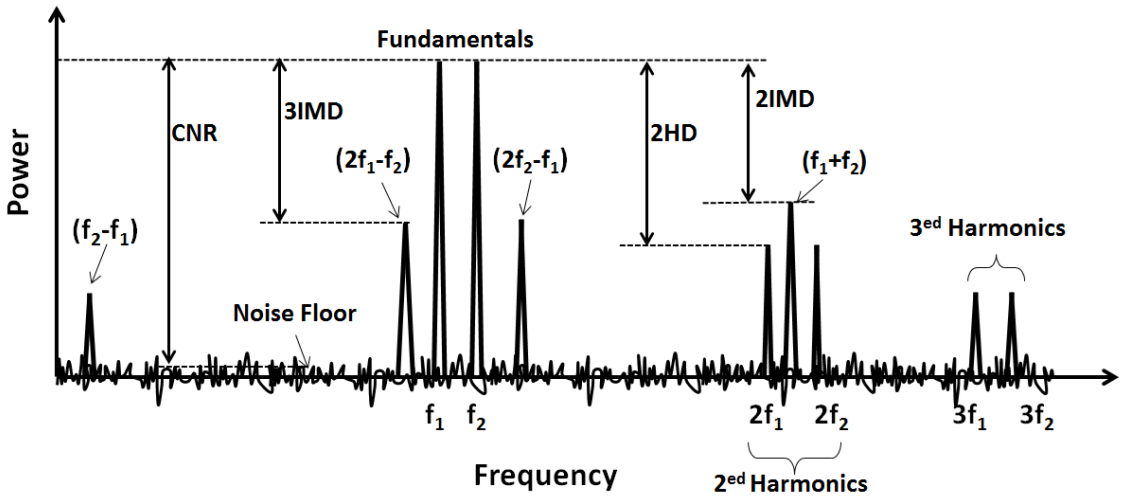

Fig. 1: Common noise and distortion products generated by nonlinear devices for two-tones.

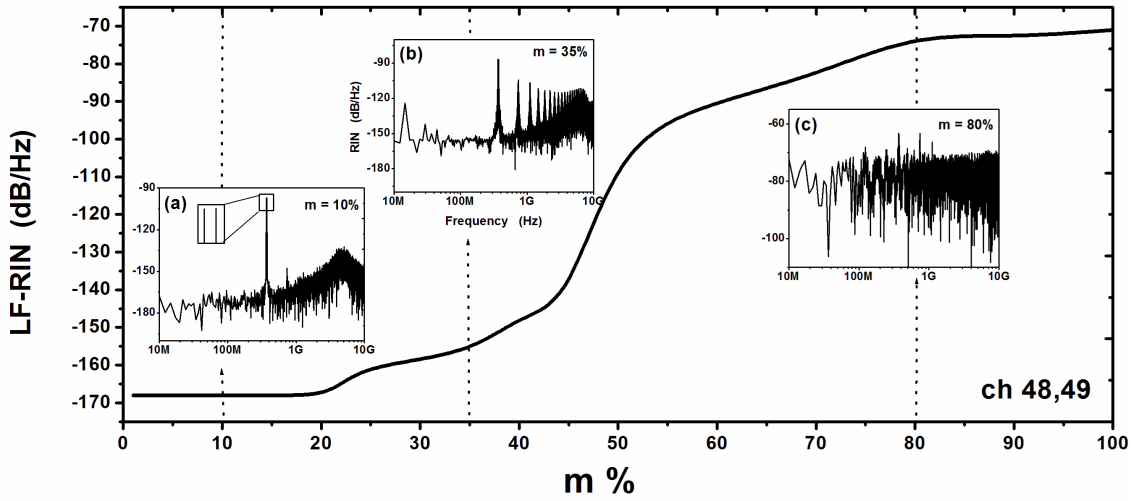

Fig. 2: Variation of LF-RIN with modulation index m under channel 48 with 49 with the simulated spectra of RIN at different modulation conditions. The LF-RIN degrades as m increase.

intermediate modulation ($m = 35\%$) and strong modulation ($m = 80\%$) with the channel frequency f_{m1}. We vary sub index between 61.25 and 547.25 MHz (ch. 3 to ch. 78) in order to cover the frequency band of the NTSC frequency plan [11]. As shown in the figure, up to $m = 20\%$ LF-RIN is constant at -168 dB/Hz regardless the value of f_{m1}. When $m = 35\%$, the LF-RIN is higher and varies with f_{m1}, but it is still within the range of the threshold acceptable values. When $m = 80\%$, the degradation in the LF-RIN level becomes as high as -80 dB/Hz, it varies within ~ 10 dB/Hz with the variation in f_{m1}.

It is interesting to examine how the laser intensity noise causes a negative impact on the CNR. Figure (4) plots variation of CNR_{RIN} (CNR degradation due to laser noise) with the modulation index m. The plots correspond to ch. 48 (f_{m1} = 367.25 MHz) and ch. 49 (f_{m2} = 373.25 MHz). We illustrate the relation between LF-RIN and CNR_{RIN} by plotting the variation of LF-RIN with m on the right-hand side axis of the figure. The figure indicates that the variation of CNR_{RIN} with m is reverse to that of LF-RIN with m. This effect is consistent with the assumption by Ahmed et al. [24] that LF-RIN is an inverse measure to the signal to noise ratio of the signal. The figure shows that up to $m = 20\%$, CNR_{RIN} increases from 55 dBc to 80 dBc, which corresponds to an increase only in the fundamental amplitude because the noise level is constant. This result agrees with measurements in [5]

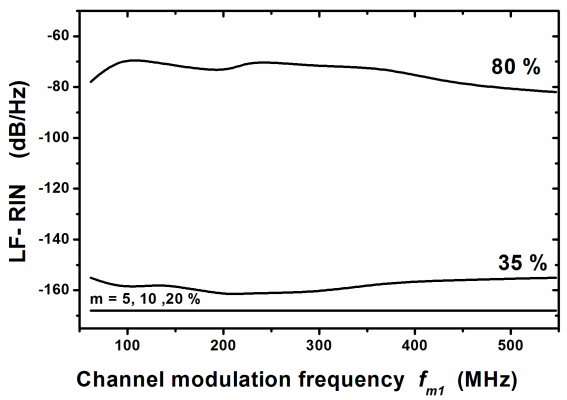

Fig. 3: Variation of LF-RIN with modulation frequency f_{m1} at different m.

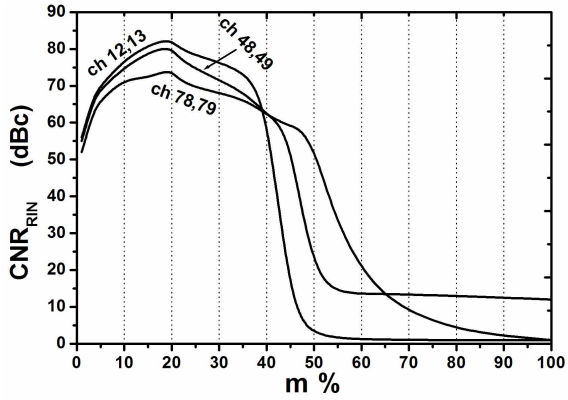

Fig. 5: Variation of CNR_{RIN} with modulation index m under channels (12 with 13), (48 with 49) and (78 with 79).

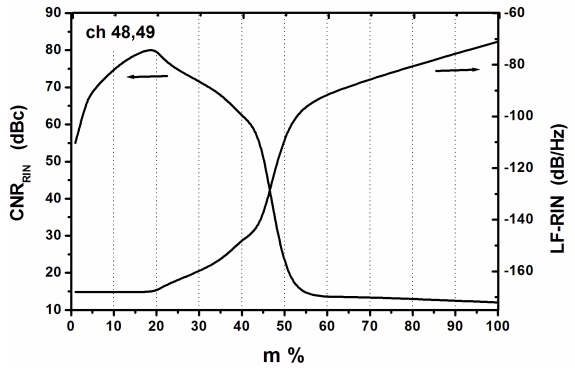

Fig. 4: Relation between LF-RIN and CNR_{RIN} under variation of m at channels 48 with 49.

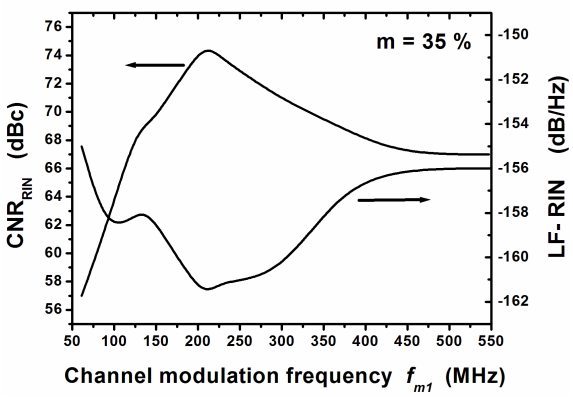

Fig. 6: Relation between CNR_{RIN} and LF-RIN under variation of modulation frequency f_{m1} when $m = 35\%$. The CNR_{RIN} levels are degrading as f_m increases beyond f_{m1} = 205.25 MHz (ch 12).

for a directly modulated 1310 nm DFB laser diode when $m \leq 15\%$ at constant LF-RIN (-150 dB/Hz). CNR_{RIN} starts to degrade when $m > 20\%$ and LF-RIN > -168 dB/Hz, which in fair agreement with the reports in [25]. When m reaches 45%, the CNR_{RIN} degradation becomes too much enhanced. We can summarize this simulation results as that, when $m \leq 20\%$ the laser intensity noise is not the dominant noise contributor to CNR.

Figure (5) compares the relation between CNR_{RIN} and m for three modulation channels; namely, ch 12 with ch. 13 (f_{m1} = 205.25 MHz and f_{m2} = 211.25 MHz), ch. 48 with ch. 49 (f_{m1} = 367.25 MHz and f_{m2} = 373.25 MHz) and ch. 78 with ch. 79 (f_{m1} = 547.25 MHz and f_{m2} = 552.25 MHz). All channels have qualitatively the same characteristics that CNR_{RIN} increases with the increase in m up to a specific value for each channel, and then degrades rapidly to unacceptable values. This specific value of m increases with the increase in the channel frequency. It is noted that the higher channel frequencies have CNR_{RIN} values worse than those of channels with lower frequencies.

As shown in figure (6), which plots CNR_{RIN} as a function of f_{m1} when $m = 35\%$, the CNR_{RIN} is maximum for ch. 12. This figure shows also that for channels below ch 12, CNR_{RIN} improves due to improvement in LF-RIN. As a numeric example, CNR_{RIN} increases from 57 dBc to 74 dBc because LF-RIN improves from -155 dB/Hz to -162 dB/Hz when f_{m1} increases from 61.25 MHz (ch. 3) to 205.25 MHz (ch. 12). At high-frequency channels, CNR_{RIN} degrades due to the increase in LF-RIN. As a numeric example, CNR_{RIN} degrades from 74 dBc to 67 dBc because LF-RIN increases from -162 dB/Hz to -156 dB/Hz when f_{m1} increases from 205.25 MHz (ch. 12) to 547.25 MHz (ch. 78).

4.2 Nonlinear distortions

The time and frequency domain investigations of 2HD, and both IMD2 and IMD3 when f_{m1} = 367.25 MHz (ch. 48) and f_{m2} = 373.25 MHz (ch. 49) for $m = 5$, 25 and

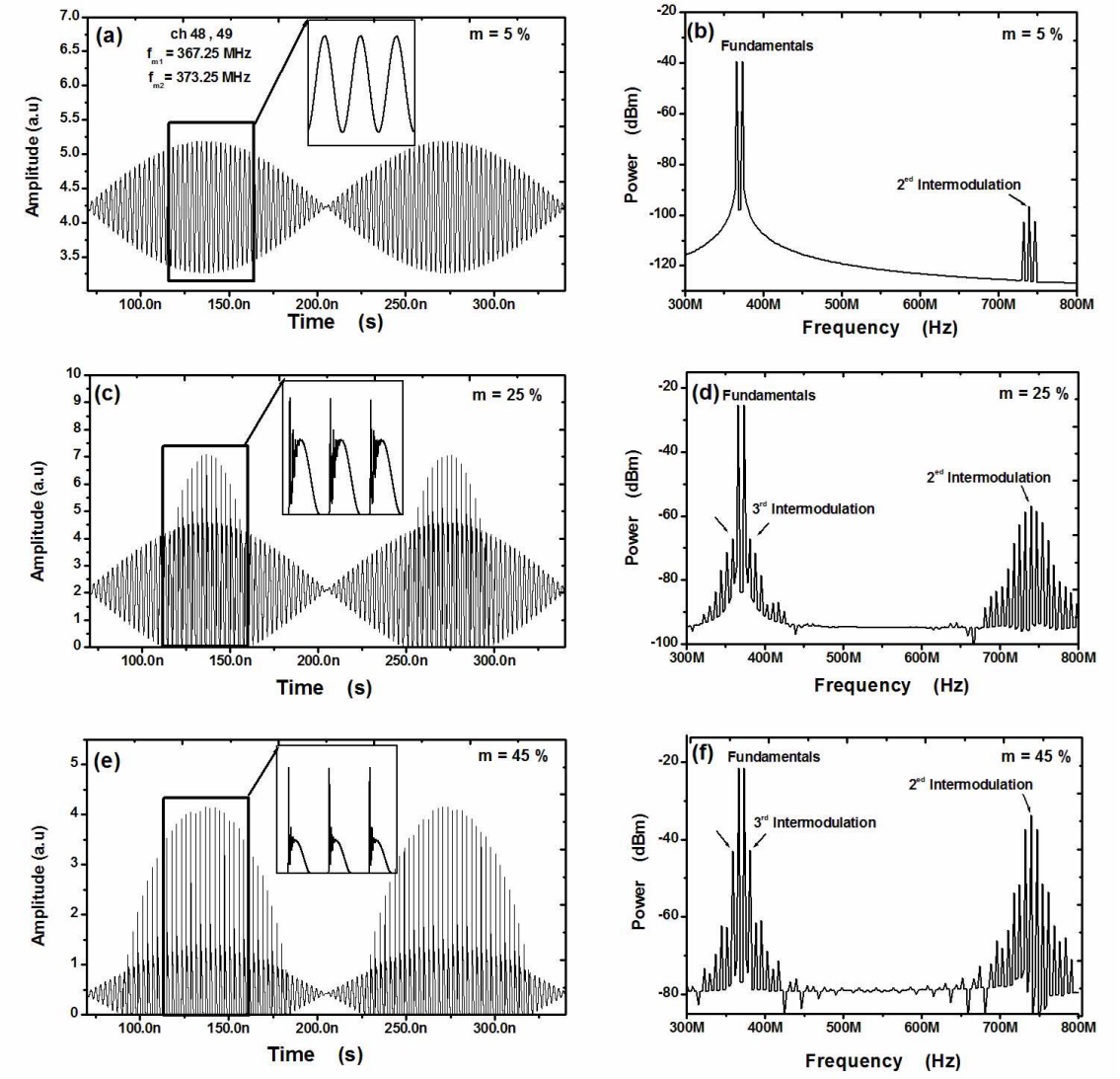

Fig. 7: Time and frequency-domain characteristics of the modulated signal under two-tone, f_{m1} =367.25 MHz (ch. 48) with f_{m2} =373.25 MHz (ch. 49) when m = 5, 25 and 45%.

45% are plotted in figure (7). Figures (7)(a), (c) and (e) illustrate the time domain presentations of the signals, while figures (7)(b), (d) and (f) plot the corresponding FFT power spectra, respectively. The time-domain figures indicate that the modulated signal distorts whenever m increases. Figure (7)(a) shows that the laser signal varies sinusoidally with the time variation, which yields lowest noise levels (-168 dB/Hz) as illustrated in figure (2). The power spectrum of figure (7)(b) has two pronounced peaks at $f = f_{m1}$ and f_{m2} (fundamentals) and other lower peaks at the higher harmonic and intermodulation components. The spectrum nearly does not display the 3rd order intermodulation products; only the 2^{ed} harmonic and 2^{ed} intermodulation products appear.

Figure (7)(c) shows that the increase in m up to 25% causes the signal to deviate from the sinusoidal form; the signal varies continuously but is clipped and superposed by sub-peaks from the relaxation oscillations of the laser in each modulation period. In figure (7)(e), both the clipping and overshoots are much stronger when m reaches 45%, which corresponds to high noise levels (-140 dB/Hz) as illustrated in figure (2). These effects can be understood as follows. The relatively large value of m exceeds the threshold current of the laser, consequently the input current drops below the laser threshold current, which then results in nearly zero output optical power and signal signal clipping. Also when $f_m \ll f_r$, the period T_m is much longer than the setting time of the relaxation

oscillations (i.e., the time instant at which the oscillations die), therefore with the instantaneous rise up of $I(t)$ the cycle duration becomes long enough to build up the relaxation oscillations in the signal. The power spectra of figures (7)(d) and (7)(f), have also pronounced two peaks at $f = f_{m1}$ and f_{m2} (fundamentals) and other lower peaks at the higher harmonic and intermodulation products. These nonlinear products carry more power as m increases, which would lead to a decrease in the difference between the fundamental power levels and consequently an increase in 2HD, IMD2 and IMD3. Figure (8)(a) illustrates the influence of m on the fundamental carrier power (assuming the two fundamental carrier power levels have the same level) as well as the nonlinear products.

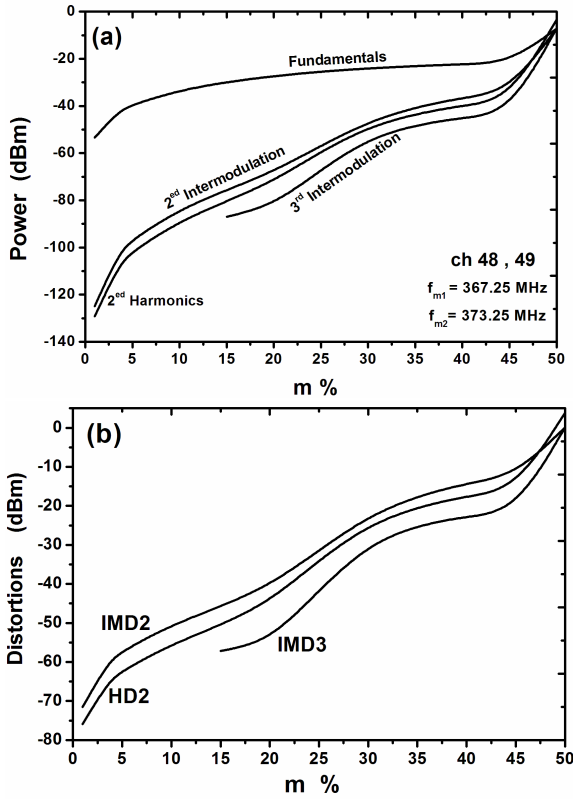

Fig. 8: Variation of (a) fundamental and nonlinear products, and (b) distortions with modulation index m at two-tone, f_{m1} =367.25 MHz (ch. 48) with f_{m2} =373.25 MHz (ch. 49).

The corresponding nonlinear distortions 2HD, IMD2 and IMD3 are plotted in figure (8)(b). The modulation conditions are similar to those of figure (2). Figure (8)(a) shows that with the increase in m, all harmonic products increase and their differences with the fundamental level diminish. The harmonic products approach the fundamental carrier (highest distortion) when $m \sim 50\%$. The 3^{rd} order intermodulation products are pronounced only when $m > 15\%$ for the relevant channels. Figure (8)(b) confirms that as m increases, all of 2HD, IMD2 and IMD3 increase. The present simulation results predict increase of both the CSO and CTB distortions with the increase in m in multichannel systems, which agree with the experimental results in [4,7,26]. Figure (7) (b) shows also that IMD2 is 4 dBm larger than 2HD, which agrees with the predictions in [18,27], and is 10 dBm larger than IMD3 which indicates an increase in the CSO distortion higher than the CTB distortion as investigated by Yonetani et al. [26]. In figure (9), we characterize 2HD, IMD2 and IMD3 when $m = 22\%$. The figure plots variation of these nonlinear distortions with the channel frequency f_{m1}. The figure indicates that all distortion types increase monotonically with the increase in f_{m1}, which predicts an increase in the CSO and CTB distortions in a multichannel system. This effect agrees with the experimental results in [7,17]. The figure indicates also that the IMD2 level is the highest, whereas the IMD3 is the lowest over the entire range of f_{m1}. The insets of the figure plot the time and frequency domain characteristics of the two-tone modulated signal at three channel placements: ch. 3 with 4 (f_{m1} = 61.25MHz and f_{m2} = 67.25MHz), ch. 42 with 43 (f_{m1} = 331.25MHz and f_{m2} = 337.25MHz), and ch. 78 with 79 (f_{m1} = 547.25MHz and f_{m2} = 553.25MHz). The insets show that the modulated signal is more distorted and the distortion products gain more power with the increase in the modulation frequency among the selected modulation channels.

4.3 Dynamic range

The dynamic range of linearity of the laser is of paramount importance for many analog modulation applications. Even if the total lasing power changes linearly with the injection current, intrinsic distortions draw power from the fundamental signal. At low modulation index m, distortions are still below the noise floor. With the increase in m, distortions rise above the noise floor and grow faster than the fundamental signal. Thus, the power level that generates distortion with amplitude equal to the noise floor is the maximum level for which the output is free from distortion. Hence this is the spur-free, or intermodulation-free, dynamic range (SFDR) [27].

Under two-tone modulation, SFDR of the laser diode is defined as the power difference between the signal and the noise floor at the point when the IMD3 power is equal to the noise floor [6]. That is, SFDR is the dynamic range of the laser when operated at the optimal modulation index m. Figure (10) plots the output power of the fundamental signal, IMD3, and noise floor versus m in the logarithmic scale at f_{m1} = 367.25 MHz (ch. 48) with f_{m2} = 373.25 MHz (ch. 49). The noise floor used in the figure is the LF-RIN, which is nearly constant at -168 dB/Hz. We estimate SFDR by linear-fitting of both the

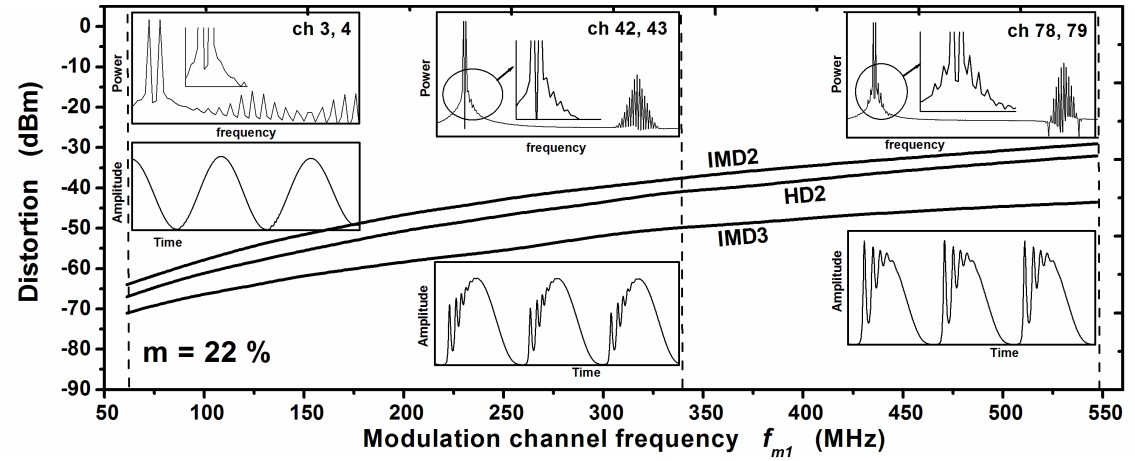

Fig. 9: Influence of modulation frequency f_{m1} on the 2HD, IMD2 and IMD3 when $m = 22\%$ with the time and frequency domain presentations at different channel placements; (3 with 4), (42 with 43) and (78 with 79). All distortion types increase as the f_{m1} increases.

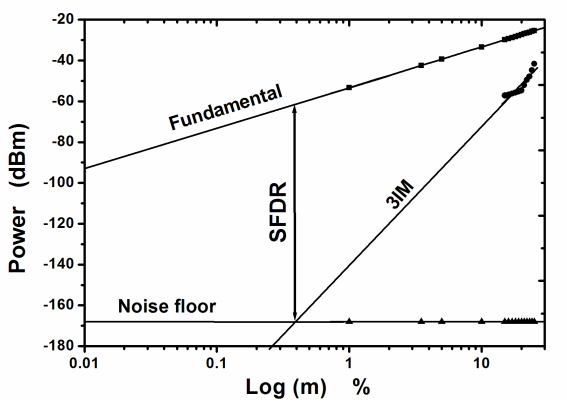

Fig. 10: SFDR determination. The fundamental tone power, 3^{rd}-order intermodulation power (3IM), and noise floor versus the modulation index *m*.

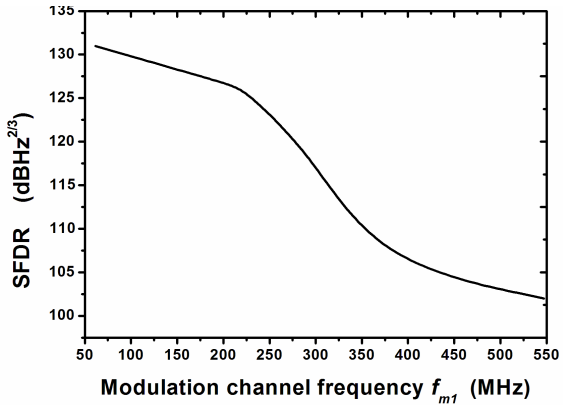

Fig. 11: Variation of SFDR with the modulation frequency f_{m1}

fundamental and the 3rd-order intermodulation powers as well as the LF-RIN level. As shown in the figure, SFDR is estimated to be 106 dBHz$^{2/3}$, which is comparable to the measured values in [6,28]. In figure (11), we illustrate the influence of the modulation channel frequency f_{m1} on SFDR. f_{m1} changes between 61.25 (ch. 3) and 547.25 MHz (ch. 78). The figure shows that SFDR decreases with the increase of f_{m1}, and ranges between 131 and 102 dBHz$^{2/3}$ over the relevant range of f_{m1}.

5 Conclusions

We introduced numerical modeling of the noise and nonlinear distortions of semiconductor lasers subjected to direct modulation with two frequencies for use in the CATV systems. The two modulation frequencies are placed according to the NTSC frequency plan of the CATV systems. The results showed that the RIN is almost constant at -168 dB/Hz in the regime of $m \leq 20\%$ regardless the value of f_m, and CNR_{RIN} increases from 52 to 80 dBc for all channels due to an increase in the fundamental amplitude. CNR_{RIN} starts to degrade when m increases beyond 20% and LF-RIN increases above -168 dB/Hz. The further increase in *m* induces much more degradation in both the noise level and the CNR_{RIN} value where the RIN has a chaos-like spectrum. In the regime of weak modulation, the signal distortion is dominated by 2HD and IMD2. The 3rd order intermodulation products

start to increase when $m > 15\%$. Under medium modulation ($m \approxeq 25\%$) the signal is clipped, and the noise level becomes too high (-140 dB/Hz). The increase in 2HD, IMD2 and IMD3 act as a robust predictor for high CSO and CTB distortions. The modulated signal waveform is more distorted and the distortion products gain more power with the increase in the channel frequency. SFDR is estimated to be 106 $dBHz^{2/3}$ which is comparable to the values reported in the literature. SFDR decreases with the increase of the channel frequency, and ranges between 131 and 102 $dBHz^{2/3}$ over the relevant range of the channel frequency.

References

[1] J. Lipson, L. Chainuluupadhyayula, S. Yuanhuang, EEC, H. B.Roxlo, E. J. Flynn, P. M. Nitzsche, C. J. Mcgrath, G. L. Fenderson,and M. S. Schaefer,*IEEE Transactions on Microwave Theory and Techniques*, **38**, 483-493, (1990).

[2] T. E. Darcie and G. E. Bodeep, *IEEE Transactions on Microwave Theory and Techniques*, **38**, 524-533, (1990).

[3] K. Y. Lau and A. Yariv, *Journal of Applied Physics Letters*, **45**, 1034-1036, (1984).

[4] H. H. Lu, Y. P. Lin, M. C. Lin,*Journal of Optical Communication*, **22**, 1-3, (2001).

[5] *Intermodulation Distortion (IMD) Measurements Using the 37300 Series Vector Network Analyzer*, **Application Note /GIP-G, Anritsu**, (2000).

[6] P. Westbergh, E. Soderberg, J.S. Gustavsson, A. Larsson, Z. Zhang, J. Berggren and M. Hammar, , **2**, 88-95, (2008).

[7] H. T. Lin and Y. H. Kao, *Journal of Lightwave Technology*, **14**, 2567-2574, (1996).

[8] A. Brillant, *Digital and analog fiber optic communications for CATV and FTTx applications*, Bellingham, Washington, USA, (2008).

[9] T. E. Darcie and G. E. Bodeep, *IEEE Journal of International Conference*, **2**, 1004-1007, (1989).

[10] W. S. Ciciora, *Cable Television in the United States* Doctorat thesis, Cable Television Labs, Inc., (1995).

[11] M. V. Water, *Low-cost CATV Transmission in Fiber-to-the-Home Networks*, Master thesis, Eindhoven University of Technology, Netherlands, (2005).

[12] H. H. Lu, C. H. Chang and P. C. Peng, *Frontiers in Guided Wave Optics and Optoelectronics*, chapter (28), Bishnu Pal (Ed.), Taiwan, (2010).

[13] Nicholas J. Frigo, Mary R. Phillips, and George E. Bodeep, *Journal of Lightwave Technology*, **11**, 138-146, (1993).

[14] S. Lai and J. Conradi, *Journal of Lightwave Technology*, **15**,20-30, (1997).

[15] M. R. Phillips and T. E. Darcie,*IEEE Journal of Photonics Technology Letters*, **3**, 1153-1155, (1991).

[16] K. Takaki, T. Kise, K. Maruyama, K. Hiraiwa, N. Yamanaka, M. Funabashi and A. Kasukawa, *High-Power CW-DFB LDs for Optical Communications* Furukawa Review, **23**, (2003).

[17] D. A. Ackemn, L. M. Zhang, J. Sheridan-Eng, E. J. Flynn and R. B. Bylsma, *IEEE, 8th Annual Meeting Conference Proceedings*, **2**, 165-166, (1995).

[18] J. Helms, *Journal of Lightwave Technology*, **10**, 1901-1906, (1992).

[19] P. J. Corvini, T.L. Koch, *Journal of Lightwave Technology*, **5**, 1591-1595, (1987).

[20] M. Ahmed, *International Journal of Numerical Modelling and Simulation* , **17**, 147-63, (2004).

[21] M. Ahmed, M. Yamada and M. Saito, *IEEE Journal of Quantum Electrons*, **37**, 1600-1610, (2001).

[22] M. Ahmed and A. Ellafi, *Journal of Optics and Laser Technology*, **40**, 809-819, (2008).

[23] M. Ahmed, N.Z. El-Sayed and H. Ibrahim, *The European Physical Journal D*, **66**, 141, (2012).

[24] M. Ahmed, A. Bakry, R. Altuwirqi, M. Alghamdi and F. Koyama, *Journal of the European Optical Society - Rapid publications*, **8**, 13064, (2014).

[25] D. Hassin and R. Vahldieck, *IEEE Transactions on Microwave Theory and Techniques*, **41**, 2376-2382, (1993).

[26] H. Yonetani, I. Ushijima, T. Takada, and K. Shima, *Journal of Lightwave Technology*, **11**, 147-153, (1993).

[27] S. C. William, *RF Photonic Technology in Optical Fiber Links*, Cambridge University Press, Cambridge, UK, (2002).

[28] H. Subbaraman, M. Yihong Chen, *IEEE/LEOS Winter Topicals Meeting Series*, 58-59, (2009).